Macromolecules

pubs.acs.org/Macromolecules Article

Enhanced Proton Selectivity in Ionomer Nanocomposites Containing Hydrophobically Functionalized Silica Nanoparticles

Allison Domhoff, Tyler B. Martin, Mayura S. Silva, Mansour Saberi, Stephen Creager, and Eric M. Davis*

Cite This: *Macromolecules* 2021, 54, 440−449

Read Online

ACCESS | Metrics & More | Article Recommendations

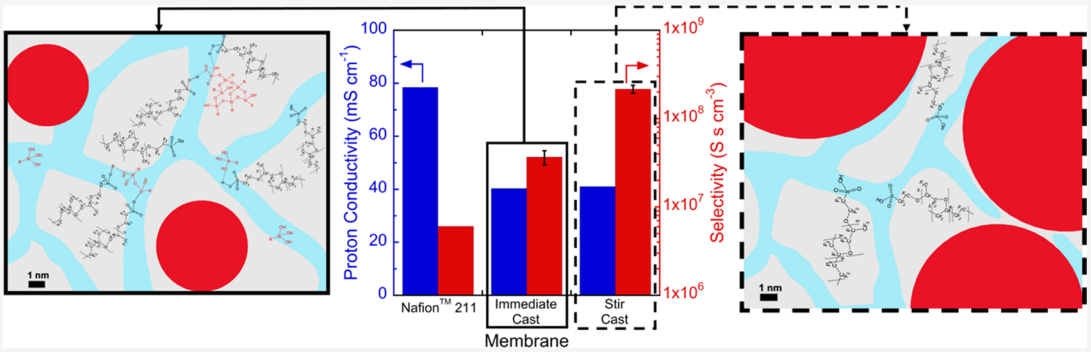

ABSTRACT: Perfluorosulfonic acid (PFSA) ionomers are ubiquitous as proton-exchange membranes (PEMs) in vanadium redox flow batteries (VRFBs), as they provide high proton conductivity and robust chemical stability. However, traditional PFSA ionomers suffer from high vanadium ion crossover, i.e., low ion selectivity, which reduces the efficiency and lifetime of the battery. Herein, a novel method to fabricate PFSA nanocomposites containing fluorocarbon-decorated silica nanoparticles is presented. These composite ionomers exhibit drastically reduced vanadium ion permeability and an almost two orders of magnitude increase in proton selectivity when compared to the current benchmark commercial ionomer. Small-angle neutron scattering data suggest that the nanostructures of these nanocomposites are drastically different from their pristine counterpart, where the periodic spacing of the hydrophobic domains is significantly reduced, while changes to the ionic structure were seen to be minimal. This work suggests that composite PEMs containing a secondary phase that alters the hydrophobic, nonion-conducting phase of the ionomer may prove to be a fruitful fabrication route to produce ionomer membranes with enhanced performance for use in VRFBs.

1. INTRODUCTION

Redox flow batteries (RFBs), and in particular vanadium redox flow batteries (VRFBs), have emerged as a viable grid-scale energy storage technology for intermittently obtained energy sources as wind and solar, providing numerous advantages over current solid-state batteries.[1−4] However, integration of RFBs into the electrical grid requires several improvements to the current technology, in particular, improvements to the ionomer membrane, which serves to physically separate the catholyte and anolyte solutions, as well as serves as a medium for facile proton transport. Perfluorosulfonic acid (PFSA) ionomers are ubiquitous in RFBs, and, in particular, Nafion[5] serves as the current benchmark material for this technology. PFSA ionomers phase-segregate under hydrated conditions into ion-conducting domains lined by sulfonic acid pendant chains and mechanically supportive hydrophobic backbone composed of poly(tetrafluoroethylene) (PTFE)-like chains.[6−8] Although Nafion exhibits high proton conductivity, the ionic network is not selective for protons, and thus, the membrane suffers from high vanadium ion crossover, which reduces the lifetime and efficiency of the VRFB.[9] To combat the low cation selectivity, several modifications to PFSA ionomer membranes have been successful including the introduction of a second phase into the ionomer, either through the incorporation of nanoparticles (NPs) or by the incorporation of another polymer through either blending or layering. However, the mechanism by which the vanadium ion transport is hindered without significantly affecting proton conductivity remains unclear.[10−13]

To date, the vast majority of modification strategies involving the introduction of a second phase into the PFSA ionomer have focused on tuning (or modifying) the electrostatic interactions of the second phase and the ionic domains

Received: July 21, 2020
Revised: December 10, 2020
Published: January 4, 2021

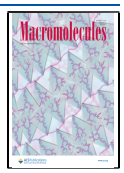

Downloaded via NATL INST OF STANDARDS & TECHNOLOGY on September 1, 2025 at 20:14:13 (UTC).
See https://pubs.acs.org/sharingguidelines for options on how to legitimately share published articles.

ACS Publications © 2021 American Chemical Society

https://dx.doi.org/10.1021/acs.macromol.0c01696
Macromolecules 2021, 54, 440−449

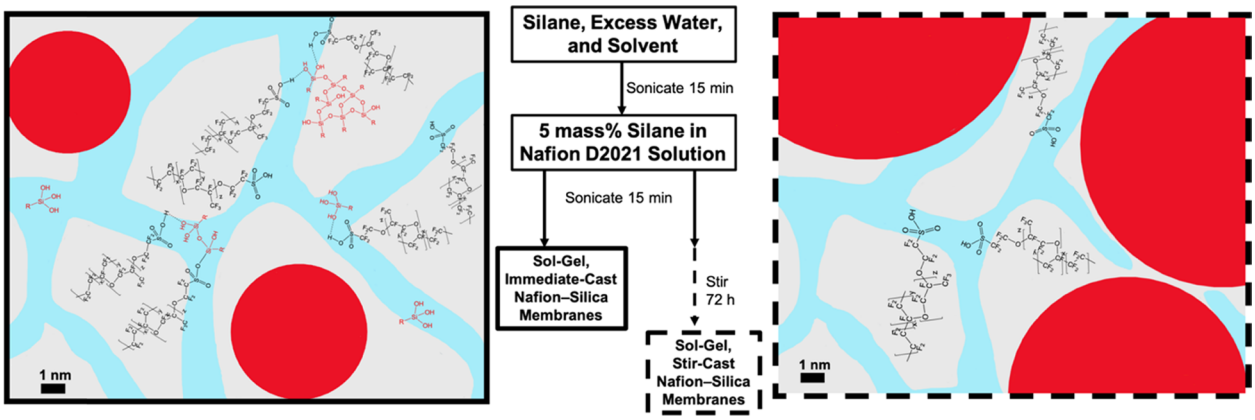

Figure 1. Sol–gel, solution casting method for the incorporation of SiNPs with varying functionality into perfluorosulfonic acid (PFSA) membranes. The illustrative schematics on the far left and far right depict the nanophase-segregated structure of Nafion, where the solid black-bordered schematic on the left is an illustration of the immediate-cast Nafion–SiNP membranes, while the dashed line bordered schematic on the right is an illustration of the stir-cast Nafion–SiNP membranes. In these schematics, the hydrophobic and hydrophilic domains are shown in gray and blue, respectively. Also, the chemical structure of Nafion is shown in black, the chemical structure of silane is shown in red, where "R" is the functional group—either –OH for TEOS or $-CH_2CH_2(CF_2)_7CF_3$ for PFTOS—and the red circles represent fully formed SiNPs. Note that the chemical structures are not drawn to scale.

of the ionomer, as it is widely accepted that the transport of water and hydrated ions occurs within these hydrophilic channels.[6,8,14] Specifically, for PFSA–SiO_2 nanocomposite membranes, it is believed that the silica nanoparticles (SiNPs) reside at least partially within the ionic domains,[15,16] reducing vanadium ion crossover by impeding the transport of bulky, hydrated vanadium ions while still providing pathways for proton transport through the ionic network.[13,15−17] Utilizing this modification strategy, a wide range of surface functionalizations of the SiNPs has been explored including hydroxyl-coated (unfunctionalized SiNPs), amine-functionalized, and sulfonic acid-functionalized.[16,18−22] In contrast, few investigations have explored the addition of a second, hydrophobic phase to improve the transport properties (and ion selectivity) of the PFSA ionomer. For example, other investigations that have blended PTFE[23] with Nafion or incorporated hydrophobic surfactants[24−26] into Nafion have demonstrated drastic reductions in vanadium ion permeability while maintaining (or even increasing) proton conductivity when compared to those of unmodified Nafion. This indicates that variations in the hydrophobic domain affect ion transport.[27−29] However, the introduction of fluorocarbon-functionalized SiNPs in proton-exchange membranes (PEMs) for VRFBs has, to the best of the authors' knowledge, never been explored.

Herein, we present a novel method to fabricate PFSA ionomer nanocomposites for vanadium redox flow batteries with superior performance properties to the current benchmark material for these applications. Specifically, our fabrication technique utilizes a combination of solution casting and sol–gel condensation chemistry to create robust PFSA–SiO_2 nanocomposite membranes that exhibit drastically improved proton selectivity (two orders of magnitude higher) when compared to the market standard, Nafion, with only a ≈50% reduction in proton conductivity for membranes with equilibrium water uptake values of around 14%. This ionomer composite is quite unique as traditional modification methods used to achieve such improved ion selectivity also result in significantly lower proton conductivities compared to unmodified PFSA ionomers.[17,20,22] Our innovative strategy combines (1) the incorporation of fluorocarbon functionality on the nanoparticle surface, allowing for better wetting of the SiNPs by the hydrophobic backbone within the ionomer, and (2) in situ sol–gel nanoparticle formation with solution casting, allowing for simultaneous nanoparticle formation and ionomer self-assembly, to create a versatile fabrication method by which the functionality of the SiNPs within the PFSA nanocomposite is easily altered through simple variation of the silane content in the initial dispersion.

2. EXPERIMENTAL SECTION

2.1. Materials. Ethanol (pure, 200 proof, anhydrous), sulfuric acid (95–98%, ACS Reagent), *N*,*N*-dimethylacetamide (DMAc) (ReagentPlus, 99%), vanadium(IV) oxide sulfate hydrate (97%), magnesium sulfate (anhydrous), 1*H*,1*H*,2*H*,2*H*-perfluorodecyltriethoxysilane (PFTOS) (97%), and tetraethyl orthosilicate (TEOS) (≥99.0%) were purchased from Sigma-Aldrich. Nafion stock dispersion (Nafion D2021) was purchased from Ion Power. Reverse osmosis (RO) water (resistivity ≈18 MΩ·cm) was used for all experiments.

2.2. Sol–Gel, Solution Casting Method. First, the silane was sonicated with excess water and solvent for 15 min, where the composition of the silane ranges from 100% TEOS to 100% PFTOS (percentages are mass % of silane). The solvent utilized in the fabrication of all ionomer nanocomposites, except those containing 100% PFTOS, was ethanol. In the case of dispersion containing 100% PFTOS, DMAc was used as the solvent. After 15 min sonication, Nafion suspension was added such that there was 5 mass % silane (based on the mass of Nafion), regardless of the silane composition. For all samples containing TEOS, the Nafion D2021 solution was added directly. For the 100% PFTOS samples, Nafion was dried out under ambient conditions and dispersed in DMAc at ≈5 mass %. The Nafion–silane mixture was sonicated again for 15 min. The samples denoted as "immediate-cast" were directly cast on polished quartz plates after the sonication. The remaining solution was stirred for 72 h before casting on polished quartz plates. These are referred to as "stir-cast" membranes. Membranes containing TEOS were dried at room temperature under a funnel with a Kimwipe-flue as previously described,[18,19] and membranes containing 100% PFTOS were dried in an oven at 80 °C under static vacuum (partial vacuum) for 30 min, dynamic vacuum for 4 h, and held at static vacuum overnight. The oven was turned off and cooled while samples were still under the vacuum. After evaporating the solvent, all of the membranes were annealed at 140 °C for 2 h (under dynamic vacuum) and then cooled to room temperature (under static vacuum), as previously

https://dx.doi.org/10.1021/acs.macromol.0c01696
Macromolecules 2021, 54, 440−449

described[18,19] and hydrated in water before permeation experiments. Note that an illustrative schematic of the sol−gel, solution casting procedure is shown in Figure 1.

2.3. Vanadium Ion Permeability Experiments. Vanadium ion crossover was measured as previously described.[18,19] Briefly, a tailor-made diffusion cell (Permegear Franz cell; Bethlehem, PA) was used; the receiving cell (volume 15 mL) was filled with 1.5 mol L^{-1} $MgSO_4$ in 3 mol L^{-1} H_2SO_4, and the donating cell (volume 1 mL) was filled with 1.5 mol L^{-1} $VOSO_4$ in 3 mol L^{-1} H_2SO_4, and the membrane was sandwiched between the two cells. Aliquots were taken via the side arm of the receiving cell at regular time intervals, and the concentration of vanadium (IV) ions (VO^{2+}; vanadyl ions) was measured using an ultraviolet−visible (UV−vis) spectrometer (VWR UV-3100PC), which scanned from wavelengths of 400 to 1100 nm. The peak associated with the presence of VO^{2+} can clearly be observed around a wavenumber of 760 nm. Immediately following UV−vis characterization, the aliquots were placed back into the receiving cell. From these data, the permeability of vanadium ions can be calculated from the following equation

$$V_R \frac{dC_R(t)}{dt} = A\frac{P}{L}C_D \tag{1}$$

where C_D and $C_R(t)$ are the vanadium ion concentrations in the donating and receiving cells (mol L^{-1}), respectively, A and L are the area (cm^2) and thickness of the membrane (cm), respectively, P is the permeability of VO^{2+} ions (cm^2 s^{-1}), and V_R is the volume of the receiving cell (L). This expression assumes the following: (1) the permeation in the membrane has reached a pseudo-steady state, (2) vanadium ion permeability is independent of ion concentration, (3) $C_D \gg C_R(t)$, and (4) the reduction in C_D over the length of the experiment is negligible.[30]

2.4. Ion-Exchange Capacity (IEC) and Water Uptake Characterization. IEC experiments were performed according to the literature.[19,31] Briefly, the membrane was dried under vacuum at 80 °C for 24 h, massed, and immersed in 1 mol L^{-1} NaCl for 24 h. Next, the membrane was removed from the NaCl solution, and the remaining solution was titrated with 0.01 mol L^{-1} NaOH with phenolphthalein (1% (by volume) in a mixture of 1:1 water/ethanol). The IEC for each membrane (mmol g^{-1}) was calculated as follows

$$\text{IEC} = \frac{V_{NaOH}C_{NaOH}}{m_{dry}} \tag{2}$$

where V_{NaOH} is the volume of the titrated NaOH solution (L), C_{NaOH} is the concentration of the NaOH solution (mmol L^{-1}), and m_{dry} is the dry mass of the membrane (g).

For water uptake experiments, the ionomer membranes were first dried under vacuum at 80 °C for 24 h. Following this drying step, the films were massed and then immediately immersed in DI water for 24 h. After 24 h, the membranes were removed, patted dry with a Kimwipe, and massed again. The following equation was used to determine the equilibrium water uptake percent

$$\text{water uptake \%} = \frac{(m_{wet} - m_{dry})}{m_{dry}} \times 100\% \tag{3}$$

where m_{wet} is the wet mass of the membrane (g).

2.5. Transmission Electron Microscopy (TEM) Imaging. TEM samples were prepared according to the literature.[18,19] Briefly, sol−gel dispersions were diluted to approximately 0.05−0.1 mass % Nafion using the same solvent as the dispersion. The dispersions were drop-cast onto 300-mesh copper grids with lacey carbon support (Electron Microscopy Services, Hatfield, PA) at the appropriate time (either immediate-cast, 15 min sonication, or stir-cast, 72 h stirring), allowed to dry in the same manner as their complementary membranes, and then annealed under the same conditions as previously described. The samples were then imaged by a Hitachi 9500 high-resolution TEM, which was operated at 300 kV, an emission current of 8.0 μA, and a filament of 29.1 V, with an exposure time of 2.0 s. ImageJ was utilized to determine particle size.[32]

2.6. Small-Angle Neutron Scattering (SANS). SANS analysis was performed at the National Institute of Standards and Technology (NIST) Center for Neutron Research (NCNR) on the NGB-10 m SANS. Nanocomposite films were cast and annealed as previously discussed, and membranes were hydrated in 100% H_2O for at least 24 h before the experiment. The hydrated films, which were on the order of 15−20 μm in thickness, were removed from the water, stacked and placed inside a demountable cell with a 2 mm gap between the quartz windows, and then sealed. Note that no additional water was added to the cell to reduce incoherent scattering from H_2O. A circular aperture with a diameter of 0.5 cm was utilized for both samples. The incoming neutron wavelength and the sample-to-detector distance were varied to collect a range of Q values ($Q = 4\pi \sin\theta/\lambda$), where θ and λ are the scattering angle and wavelength of the neutrons, respectively. In this study, SANS data were collected over Q values ranging from 0.0035 to 0.5 $Å^{-1}$. The SANS data were reduced using the software package developed at the NIST Center for Neutron Research,[33] where the thickness of the cell was used for all reduction calculations.

2.7. Proton Conductivity and Selectivity. All of the membranes were pretreated prior to obtaining conductivity measurements. Membranes were initially immersed in 3% H_2O_2 solution at 70 °C for 1 h, and then after a brief wash with DI water, membranes were soaked in 0.5 mol L^{-1} H_2SO_4 solution at 70 °C for 1 h. Membranes were then washed again and stored in DI water prior to use in conductivity measurements. Based on previous methods,[34,35] a miniature electrochemical cell based on a modified plastic compression fitting was used to obtain through-plane ionic conductivity measurements on membranes. Electrodes having 2 mg cm^{-2} Pt/C (Pt on carbon cloth, Fuel Cell Store) were attached onto graphite rods (current collectors), and the graphite rods were pressed onto the membrane surface to define an active electrode area of 0.178 cm^2. Each side of the cell was bathed with humidified hydrogen gas, and symmetrical electrochemical hydrogen pump experiments were carried out on membranes at a 100% relative humidity and at room temperature, which provided linear current−voltage curves reflecting proton transmission rates through the membranes. A WaveDriver 20 potentiostat/galvanostat system (Pine Research Instrumentation) was utilized for data collection, and AfterMath data organizer software (Pine Research) was utilized to analyze the data. Membrane resistance was calculated from the inverse slope of linear current−voltage curves, and conductivity was obtained from resistance by accounting for geometric factors (area and thickness).

From the proton conductivity and vanadium ion permeability, proton selectivity for membranes can be calculated as follows

$$S = \frac{\sigma}{P} \tag{4}$$

where S (S s cm^{-3}) is the proton selectivity, σ (mS cm^{-1}) is the proton conductivity, and P (cm^2 s^{-1}) is the vanadium ion permeability (analogous to that defined above).

3. RESULTS AND DISCUSSION

3.1. Membrane Preparation. Figure 1 depicts the general procedure for the sol−gel, solution casting fabrication technique, along with an illustrative schematic of the theoretical structures of the nanocomposites formed by two fabrication avenues. In this figure, the PFSA ionomer chemical structure is shown in black, with the hydrophobic domain shaded in gray and the hydrophilic domain shaded in blue. The silane functionality in the chemical structure has been colored red. The SiNPs (red circles in the schematic on the right) or SiNP precursors (chemical structure in the schematic on the left) are shown in red, where R represents the specific silane functionality (either −OH for tetraethyl orthosilicate (TEOS) or $-CH_2CH_2(CF_2)_7CF_3$ for 1*H*,1*H*,2*H*,2*H*-perfluorodecyltriethoxysilane (PFTOS)). Briefly, the silane was sonicated with excess water and solvent (either ethanol or DMAc) for 15 min. Next, the Nafion dispersion was added to the silane solution

https://dx.doi.org/10.1021/acs.macromol.0c01696
Macromolecules 2021, 54, 440−449

Table 1. Vanadyl Ion (VO^{2+}) Permeability, IEC, and Equilibrium Water Uptake of Sol−Gel, Solution-Cast PFSA Ionomer Nanocomposites with Various Silane Compositions[a]

	immediate-cast			stir-cast		
composition of silane	VO^{2+} permeability (10^{-9} cm^2 s^{-1})	IEC (mequiv g^{-1})	water uptake (%)	VO^{2+} permeability (10^{-9} cm^2 s^{-1})	IEC (mequiv g^{-1})	water uptake (%)
100% TEOS	6.0 ± 0.4	0.877 ± 0.006	17.1 ± 1.5	5.5 ± 0.3	0.934 ± 0.004	17.5 ± 3.6
50% TEOS−50% PFTOS	5.2 ± 0.4	0.87 ± 0.01	17.0 ± 0.8	5.7 ± 0.5	1.1 ± 0.2	9.9 ± 0.9
25% TEOS−75% PFTOS	3.4 ± 0.5	0.85 ± 0.06	18.4 ± 1.0	5.7 ± 0.3	1.001 ± 0.002	11.9 ± 4.1
100% PFTOS	1.1 ± 0.2	0.87 ± 0.01	5.2 ± 0.9	0.19 ± 0.02	0.8 ± 0.1	13.8 ± 3.9

[a]The error is given as the standard deviation of the average based on triplicate experiments.

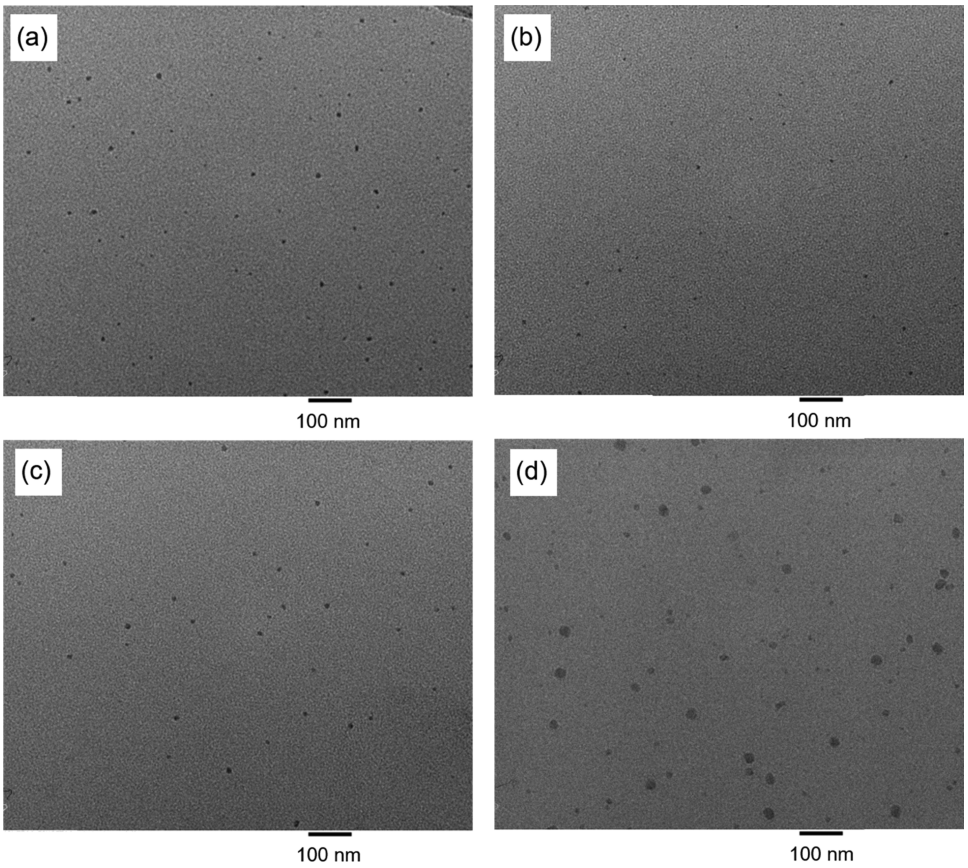

Figure 2. TEM images of immediate-cast sol−gel, solution-cast membranes with (a) 100% TEOS, (b) 50% TEOS−50% PFTOS, (c) 25% TEOS−75% PFTOS, and (d) 100% PFTOS. All scale bars are 100 nm in length, and magnification for (a)−(d) is 40 000×.

such that there was 5 mass % silane to the mass of the Nafion solids, after which the dispersion was further sonicated for 15 min to ensure adequate mixing. The membranes noted as immediate-cast were cast onto polished quartz plates immediately after the 15 min sonication cycle. The theoretical schematic of the immediate-cast membrane is shown in Figure 1 with a solid border. The membranes noted as stir-cast were stirred for 72 h after the initial sonication cycle before being cast onto polished quartz plates. The theoretical schematic of the stir-cast membrane is shown in Figure 1 with a dashed border. All membranes were further annealed at 140 °C for 2 h under dynamic vacuum and cooled to room temperature under static vacuum as previously described.[18,19] In this work, we prepared composites using both fabrication routes and at varying silane compositions (by mass %) of 100% TEOS, 50% TEOS−50% PFTOS, 25% TEOS−75% PFTOS, and 100% PFTOS. Note that the listed mass % are with respect to the silane mass only, where the total amount of silane with respect to the amount of PFSA ionomer is held constant (at 5 mass %) across all membranes. More detailed information regarding the sol−gel solution casting procedure can be found in the Experimental Section.

3.2. Vanadyl Ion Permeability and TEM Imaging. Table 1 shows the vanadyl ion (VO^{2+}) permeability, ion-exchange capacity (IEC), and water uptake for all of the ionomer nanocomposite membranes. As seen in Table 1, reduced VO^{2+} permeability was observed for all membranes, both immediate-cast and stir-cast, when compared to Nafion 211 membranes, the current benchmark material for VRFBs. Note that the VO^{2+} permeability of Nafion 211 was calculated to be 13×10^{-9} cm^2 s^{-1}, which falls within the range of permeabilities reported in the literature.[36,37]

To complement the performance data highlighted in Table 1, transmission electron microscopy (TEM) images of both the

https://dx.doi.org/10.1021/acs.macromol.0c01696
Macromolecules 2021, 54, 440−449

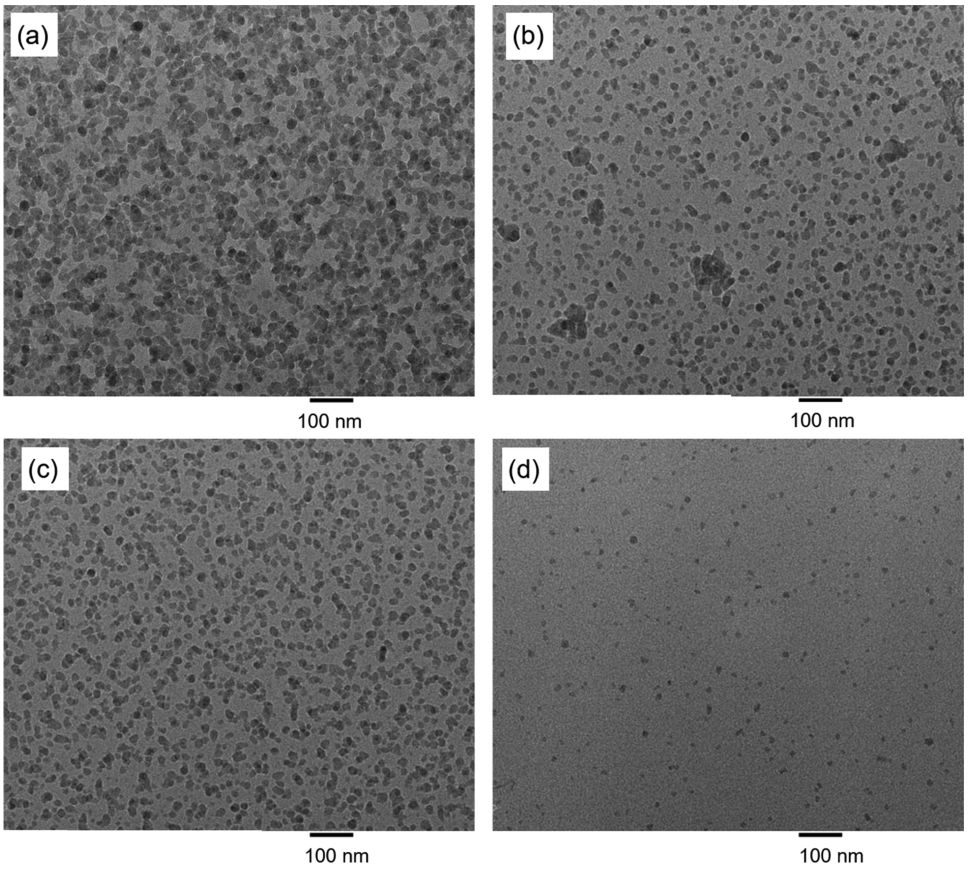

Figure 3. TEM images of stir-cast sol−gel, solution-cast membranes with (a) 100% TEOS, (b) 50% TEOS−50% PFTOS, (c) 25% TEOS−75% PFTOS, and (d) 100% PFTOS. All scale bars are 100 nm in length, and magnification for (a)−(d) is 40 000×.

immediate-cast and stir-cast series of membranes were captured and are shown in Figure 2. Focusing our attention on the immediate-cast membranes (Figure 2a−d), we see that all of the TEM images depict small NPs on the order of ≈5 nm in diameter, as determined by ImageJ (NIH software, particle size analysis), that are well dispersed within the PFSA ionomer. The membranes fabricated with 100% PFTOS exhibited slightly larger particles, on average, but were still all 10−20 nm in diameter. While the SiNP dispersion state does not drastically change with silane concentration, the VO^{2+} permeability of these films is drastically different. As seen in Table 1, the incorporation of fluorocarbon functionality on the SiNPs, and the remaining silane, through increasing concentrations of PFTOS further reduces the vanadium ion permeability. The incorporation of just 50% PFTOS reduces the vanadium ion permeability by ≈60%, as compared to that of Nafion 211, without significantly affecting the IEC of the membrane (0.87 ± 0.01 mequiv g^{-1}). The IEC of a membrane is a measure of the mols of (accessible) sulfonic acid groups per dry mass of the composite polymer membrane, and for nanocomposite membranes, variations in IEC compared to those of the pristine PFSA ionomer indicate variations in the formation of the ionic domains. The incorporation of 75% PFTOS and only 25% TEOS should yield more fluorocarbon functionality within the nanocomposite, and the vanadium ion permeability of these membranes is even further reduced, by ≈75% as compared to that of Nafion 211, with again, similar IEC values (0.85 ± 0.06 mequiv g^{-1}) and equilibrium water uptake (18.4 ± 1.0%) to the other immediate-cast nanocomposite membranes.

The largest reduction in vanadium ion permeability was observed for those membranes fabricated with 100% PFTOS ((1.11 ± 0.2) × 10^{-9} cm^2 s^{-1}), a reduction of over 90% when compared to that for Nafion 211 membranes. As mentioned above, the TEM image for these membranes (Figure 2d) shows well-dispersed fluorocarbon-decorated SiNPs, with slightly larger diameters than those seen in the TEM images for the other immediate-cast membranes (Figure 2a−c). As mentioned in the Experimental Section, the formation of the sol−gel, solution-cast membranes with 100% PFTOS required the use of higher-boiling-point solvent dimethylacetamide (DMAc), and thus, the film formation occurred at high temperature to evaporate the solvent. The larger sizes of the fluorocarbon-decorated SiNPs likely occur due to this increased temperature of casting, which accelerates the rate of silane hydrolysis and SiNP growth, allowing the NPs to nucleate and quickly form larger fluorocarbon-decorated SiNPs before the solvent is fully evaporated. Interestingly, the IEC of the 100% PFTOS immediate-cast membranes is similar to the rest of the immediate-cast membranes, suggesting that the same number of sulfonic acid groups within Nafion are available for ion exchange and proton conduction in all of the immediate-cast membranes, regardless of silane composition. However, the water uptake of the immediate-cast 100% PFTOS membranes (5.2 ± 0.9) is significantly reduced compared to that of not only Nafion 211 but also the other immediate-cast membranes with a lower concentration of PFTOS.

Focusing our attention on the stir-cast series of PFSA ionomer nanocomposites, we observe that the SiNP nucleation

https://dx.doi.org/10.1021/acs.macromol.0c01696
Macromolecules 2021, 54, 440−449

and growth that occur when the dispersions are allowed to stir 72 h are quite drastic, as seen in the TEM images of the stir-cast sol−gel, solution-cast membranes shown in Figure 3a−d. Comparing the TEM images of the immediate-cast and stir-cast series of membranes, it becomes evident that the immediate-cast series of membranes contained a large amount of unreacted silane or silane oligomers. That is, given the small number of observable fully formed SiNPs by TEM in the immediate-cast films, as compared to the amount shown in the stir-cast series, it becomes clear that the majority of the silane precursor was not used in the formation of SiNPs. Figure 3a shows that the silane in the 100% TEOS stir-cast film has all nucleated and formed SiNPs of similar sizes, ranging approximately 15−30 nm in diameter, with large aggregates that span the entire TEM image. However, the introduction of fluorocarbon-decorated SiNPs through the incorporation of PFTOS changes the nanoparticle dispersion state, as well as the number of fully formed NPs visible in the TEM images (Figure 3b−d). Note that while the composition of the silane is based on a mass % calculation, the molar mass of PFTOS is approximately 3 times the molar mass of TEOS; therefore, membranes containing the same mass of 100% TEOS and 100% PFTOS have different mols of Si that can contribute to forming the SiNPs. This means that the number of NPs formed will not necessarily be the same in membranes containing various compositions of silane, with the amount of SiNPs formed being least in membranes containing 100% PFTOS, which can be observed in Figure 3d in comparison to Figure 3a−c.

Additionally, as the concentration of PFTOS is increased, the surface of the NPs becomes more densely decorated with bulky fluorocarbon groups, which lead to a better NP dispersion state (i.e., increased dispersion of the SiNPs within the ionomer nanocomposite), with the most homogeneous dispersion observed for 100% PFTOS stir-cast membranes. As seen in the TEM image in Figure 3d, stir-cast membranes with 100% PFTOS have a greater number (i.e., higher concentration) of smaller diameter particles when compared to their immediate-cast counterpart (Figure 2d). The high temperature required for the solvent evaporation of these membranes, as described in the Experimental Section, increases the reactivity of the silane to form SiNPs faster, but we hypothesize that the extended stirring time that the silane is in the polymer solution allows all PFTOS to be used, creating more but slightly smaller particles. It is clear from these TEM images that the long fluorocarbon functionality on the fluorocarbon-decorated SiNPs minimizes aggregation, and favorable wetting is promoted between the fluorocarbon functionality of the SiNPs and the PTFE-like backbone of the PFSA ionomer (Figures 2d and 3d).

As seen in Table 1, the VO^{2+} permeabilities of the stir-cast membranes fabricated using any amount of TEOS are similar to each other, as well as similar to the immediate-cast 100% TEOS membranes. Additionally, the IEC values of stir-cast membranes fabricated with 25−100% TEOS are all similar to that of the IEC of Nafion 211 (IEC = 0.95−1.01 mequiv g^{-1}).[38] The water uptake values for all stir-cast membranes vary from their immediate-cast counterparts, likely due to the difference in particle size and dispersion, affecting the ionic domain formation, even at the same initial silane compositions. The most dramatic reduction in VO^{2+} ion permeability was observed for 100% PFTOS stir-cast membranes with almost 2 orders of magnitude reduction in VO^{2+} permeability ((0.19 ± 0.02) × 10^{-9} cm^2 s^{-1}), while only an ≈20% reduction in IEC (0.8 ± 0.1 mequiv g^{-1}), when compared to that of Nafion 211, was observed.[38] Further, the VO^{2+} permeability of the stir-cast membranes with 100% PFTOS is also 1 order of magnitude lower than its immediate-cast counterpart. The introduction of fluorocarbon-decorated SiNPs into the Nafion nanocomposite at all concentrations for immediate-cast and at 100% PFTOS stir-cast reduced the vanadium ion permeability more than either typical solution-cast or sol−gel solution-cast with unfunctionalized SiNPs.[10,19,39]

3.3. Small-Angle Neutron Scattering. From the results thus far, the two most promising membranes fabricated have been the immediate-cast and stir-cast 100% PFTOS membranes, as both membranes have exhibited the highest reduction in VO^{2+} permeability, with relatively small reductions in IEC. Further, as seen from the TEM images of these two membranes (see Figures 2d and 3d), both exhibit similar fluorocarbon-decorated SiNP dispersion states, though overall, the stir-cast membranes have a higher concentration of NPs. To help elucidate the structural differences between these two membranes, small-angle neutron scattering (SANS) experiments were performed. The SANS curves of 100% PFTOS immediate-cast and stir-cast membranes, both hydrated before analysis, are shown in Figure 4. Interestingly,

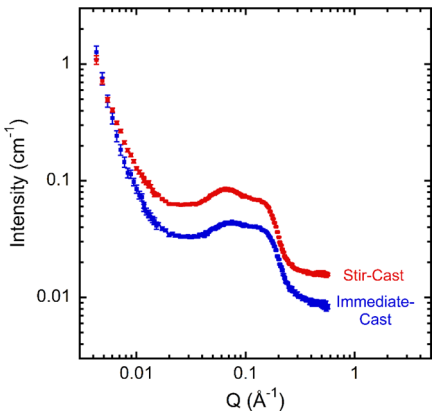

Figure 4. Small-angle neutron scattering (SANS) curves of 100% PFTOS immediate-cast (close blue) and 100% PFTOS stir-cast (closed red) membranes. The membranes were hydrated in 100% H_2O for 24 h before analysis; however, no additional water was added to the cell when mounting the membrane. All SANS experiments were performed at room temperature.

the two characteristic Nafion scattering peaks[40,41]—a low-Q peak associated with the periodic (center-to-center) spacing of the PTFE-like domains (hydrophobic domains; referred to as the hydrophobic/crystalline peak), as well as a high-Q peak associated with the periodic spacing of the coalesced ionic groups (hydrophilic (ionic) domains; oftentimes referred to as the ionomer peak)—have both shifted so much that they are now overlapping with each other. We believe this shift of the peaks is caused by the presence of the hydrophobically coated SiNPs and is not an effect of the solvent used in the preparation of these solution-cast membranes. As mentioned above, membranes prepared with 100% PFTOS were cast from a dispersion of Nafion in DMAc and not from ethanol, like all of the other ionomer nanocomposites in this study. However, previous research has shown that the hydrated nanostructures of pristine Nafion membranes solution-cast from either DMAc or ethanol (specifically a 4:1 mixture (by mass) of ethanol and

https://dx.doi.org/10.1021/acs.macromol.0c01696
Macromolecules 2021, 54, 440−449

water) are similar,[42] suggesting that the altered nanostructures we observe in the SANS data are directly related to the formation and presence of the fluorocarbon-coated SiNPs and not to the specific solvent used in the membrane fabrication process. Similar to previously synthesized PFSA ionomer nanocomposites,[10,18] those created by sol−gel, solution casting with 100% PFTOS also exhibit a low-Q upturn, where the slope of this low-Q upturn for both nanocomposite membranes investigated is similar. This low-Q upturn is indicative of larger structures within the nanocomposite membrane and is often attributed to SiNP aggregation.[18,43] The center-to-center spacing of the hydrophilic and hydrophobic domains can be correlated from the Q positions of these two peaks, Q^*, where the d-spacing, $d = 2\pi/Q^*$, was calculated from the local maxima for each peak. The results of this analysis are summarized in Table 2. Note that the peak maxima were estimated by visual examination of the scattering curves.

Table 2. SANS Peak Positions and Bragg d-Spacing of 100% PFTOS Membranes

composition of silane	peak position ($Å^{-1}$)		d-spacing (nm)	
	hydrophobic	hydrophilic	hydrophobic	hydrophilic
solution-cast Nafion[a]	0.0584	0.141	10.8	4.45
100% PFTOS immediate-cast	0.0804	0.135	7.81	4.65
100% PFTOS stir-cast	0.0748	0.135	8.40	4.65

[a]Previously published by Domhoff et al.[18]

For comparison, the d-spacing of the hydrophobic and hydrophilic domains of hydrated, solution-cast pristine Nafion is listed in Table 2.[18] As seen from Table 2, the introduction of the fluorocarbon-decorated SiNPs by sol−gel, solution casting, for either the stir-cast or the immediate-cast membranes, the spacing between hydrophobic domains is reduced by ≈22% and ≈28%, respectively. Additionally, the spacing between ionic domains increases marginally for both immediate-cast and stir-cast membranes by ≈5% increase compared to that of pristine Nafion. The reduction in spacing of the hydrophobic domains supports our hypothesis that the PTFE functionality on the SiNPs surface allows for better wetting of the NPs by the PTFE-like backbone of the PFSA ionomer. Interestingly, the spacing between hydrophobic domains for the 100% PFTOS immediate-cast membranes is less than that of the 100% PFTOS stir-cast membranes (7.81 nm vs 8.40 nm). We postulate that the higher concentration of unreacted silanes in the immediate-cast membranes can more easily maneuver within the ionomer matrix as crystallization occurs during thermal annealing, creating tighter packing and thus reduced spacing between hydrophobic domains.

As previously mentioned, it has been traditionally assumed that the observed reduction in vanadium ion crossover in these PFSA ionomers was a result of the NPs residing at least partially within the ionic domains of the ionomer, physically blocking the bulky, hydrated vanadium ions from transporting across the membrane. For this reason, the majority of investigations targeted at altering the ion selectivity of these membranes have focused their efforts on altering the electrostatic interactions between the NP surface and the sulfonic acid groups that coalesce to form channels for facile ion transport.[11,16,20,31,36] However, as seen from the SANS data of these hydrated membranes in Figure 4, the introduction of the fluorinated NPs actually acts to more significantly alter the structure and spacing of the PTFE-like domains, demonstrating that substantial changes in vanadyl permeability can be achieved without drastically altering the ionic morphology of the membrane. While vanadium ion permeability is a property of merit for the use of these ionomers in VRFBs, more important performance properties are proton conductivity and ion selectivity (i.e., proton conductivity/VO^{2+} permeability), which are directly tied to the coulombic and voltage efficiencies of VRFBs. Therefore, the proton conductivity of the 100% PFTOS immediate-cast and stir-cast membranes, along with the benchmark membrane, Nafion 211, was measured.

3.4. Proton Conductivity. The proton conductivity (solid blue bar) and ion selectivity (solid red bar) of Nafion 211, 100% PFTOS immediate-cast, and 100% PFTOS stir-cast membranes are shown in Figure 5. The values obtained for the

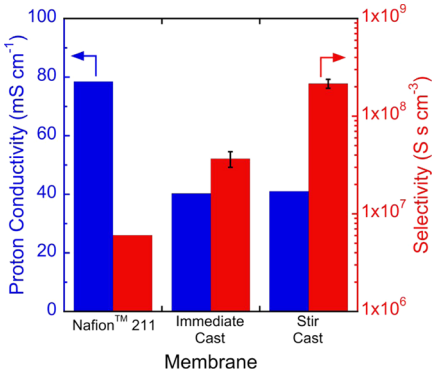

Figure 5. Proton conductivity (blue bars, left y-axis) and selectivity (red bars, right y-axis) of Nafion 211, 100% PFTOS immediate-cast, and 100% PFTOS stir-cast membranes. Note that error bars on the selectivity calculations result from the propagation of uncertainty from repeat vanadium (vanadyl) ion permeation experiments.

proton conductivity and ion selectivity of Nafion 211 are consistent with those reported in the literature, where the low ion selectivity of these membranes underscores the need to develop next-generation membranes with improved performance.[37] Additionally, as mentioned in the Experimental Section, the conductivity of these membranes was obtained utilizing humidified (saturated) hydrogen, which differs from the acidic electrolytes the membrane would encounter within an operating VRFB, where under these acidic conditions, conductivities have been previously measured to be slightly lower than those measured in pure water.[44−46] As seen in Figure 5, the introduction of fluorocarbon-decorated SiNPs in both the 100% PFTOS immediate-cast and stir-cast membranes results in a reduction of the conductivity to a value that is approximately half that of the benchmark, Nafion 211, though this value is sufficient for operation in RFBs.[47] However, when we look at the ion selectivity of the two 100% PFTOS membranes, we observe that the ion selectivity of nanocomposite membranes is significantly higher than that of Nafion 211. Most notably, the 100% PFTOS stir-cast membranes, which exhibited a 99+% reduction in VO^{2+} ion permeability (0.11×10^{-9} vs 13×10^{-9} cm^2 s^{-1}), have an ion selectivity that is almost two orders of magnitude higher than that of Nafion 211 ($\approx 2 \times 10^8$ vs $\approx 6 \times 10^6$ S s cm^{-3}). Given

https://dx.doi.org/10.1021/acs.macromol.0c01696
Macromolecules 2021, 54, 440−449

this significant increase in proton selectivity, we believe that our novel fabrication method presents an avenue to create feasible alternatives for traditional PEMs for VRFBs, as this method can be utilized with more cost-effective materials like sulfonated polystyrenes and poly(aryl ether ketone)s.

We believe that the observed increase in membrane performance occurs due to the presence of fluorocarbon-decorated SiNPs in the hydrophobic domain, which is potentially twofold: (1) the introduction of fluorocarbon-decorated SiNPs into the ionomer results in an overall increase in the tortuosity of the ionic channels without significantly impacting the size/period spacing of the ionic domains (i.e., impacts to ionomer self-assembly) and (2) the introduction of fluorocarbon-decorated SiNPs into the ionomer acts to slow down the segmental chain dynamics of the fluorocarbon backbone of the ionomer due to favorable wetting of the NP surface by the PTFE-like ionomer backbone. We postulate that the fluorocarbon-decorated SiNPs tether the fluorocarbon groups of Nafion, which acts to impede the otherwise peristaltic-like motions of the backbone that facilitate water and ion transport through the hydrated membranes.[48−50] Peristaltic-like motions that encourage facile ion transport were first proposed by Di Noto et al.,[49] where the proton hopping transport mechanism that occurs through the ionic domains is caused by a combination of effects in both the ionic domain and backbone within Nafion. The factors that influence the peristaltic-like motions include the interstitial free water in the ionic domains, the sequestration of sulfonic acid sites in the ionic domain by the introduction of SiNPs, and the segmental chain dynamics of the fluorocarbon backbone.[48−50]

4. CONCLUSIONS

In conclusion, we have successfully fabricated PFSA ionomer nanocomposites via sol−gel, solution casting with varying amounts of fluorocarbon-decorated SiNPs, some of which are suitable for use in commercial VRFBs. Specifically, the introduction of SiNPs in the series of immediate-cast membrane resulted in a reduction in the vanadyl ion permeability with increasing PFTOS composition, without affecting the IECs of the resulting membranes. For films with some amount of TEOS, the TEM images suggest that most of the silane does not contribute to the formation of SiNPs but forms small oligomers that are not visible by TEM imaging. All of the stir-cast sol−gel, solution-cast membranes containing TEOS have similar vanadyl ion permeabilities, where IECs for these membranes were similar to that of Nafion 211. The TEM images of these membranes indicated that the SiNPs tended to aggregate, but the diameter of the NPs did not significantly change across the varying silane compositions. Notably, the highest reduction in VO^{2+} ion permeability occurred for the samples containing 100% PFTOS, for both the immediate-cast and stir-cast membranes, where an almost 2 orders of magnitude reduction in vanadyl ion permeability was observed for the 100% PFTOS stir-cast membranes. The TEM images for both membranes showed well-dispersed particles with little aggregation, though the concentration of fully formed NPs was higher for the 100% PFTOS stir-cast membranes. The proton conductivity of the immediate-cast and stir-cast membranes with 100% PFTOS is approximately half that of Nafion 211, though still suitable for commercial VRFBs; however, the proton selectivity increased almost one and two orders of magnitude, respectively. These results underscore the role of the PTFE-like, hydrophobic domain in governing ion transport through these PFSA ionomer nanocomposites.

■ AUTHOR INFORMATION

Corresponding Author

Eric M. Davis − *Department of Chemical and Biomolecular Engineering, Clemson University, Clemson, South Carolina 29634, United States;* orcid.org/0000-0002-5633-5489; Email: ericd@clemson.edu

Authors

Allison Domhoff − *Department of Chemical and Biomolecular Engineering, Clemson University, Clemson, South Carolina 29634, United States;* orcid.org/0000-0002-0264-0410

Tyler B. Martin − *National Institute of Standards and Technology (NIST), Gaithersburg, Maryland 20899, United States;* orcid.org/0000-0001-7253-6507

Mayura S. Silva − *Department of Chemistry, Clemson University, Clemson, South Carolina 29634, United States;* orcid.org/0000-0002-3708-950X

Mansour Saberi − *Department of Chemical and Biomolecular Engineering, Clemson University, Clemson, South Carolina 29634, United States*

Stephen Creager − *Department of Chemistry, Clemson University, Clemson, South Carolina 29634, United States;* orcid.org/0000-0002-7412-2268

Complete contact information is available at: https://pubs.acs.org/10.1021/acs.macromol.0c01696

Notes

The authors declare no competing financial interest.

■ ACKNOWLEDGMENTS

The authors gratefully acknowledge partial support from the National Science Foundation CAREER program (DMR-1848347) and the Clemson University Advanced Materials Research Lab for use of their electron microscopy facilities. A.D. would like to acknowledge the support of the National Science Foundation Graduate Research Fellowship Program (award no. 1246875) and the Hitachi High Technologies Electron Microscopy Graduate Fellowship.

■ REFERENCES

(1) Skyllas-Kazacos, M.; Kazacos, M. State of Charge Monitoring Methods for Vanadium Redox Flow Battery Control. *J. Power Sources* **2011**, *196*, 8822−8827.

(2) Skyllas-Kazacos, M.; Kasherman, D.; Hong, D. R.; Kazacos, M. Characteristics and Performance of 1 KW UNSW Vanadium Redox Battery. *J. Power Sources* **1991**, *35*, 399−404.

(3) Cunha, Á.; Martins, J.; Rodrigues, N.; Brito, F. P. Vanadium Redox Flow Batteries: A Technology Review. *Int. J. Energy Res.* **2015**, *39*, 889−918.

(4) Gallo, A. B.; Simões-Moreira, J. R.; Costa, H. K. M.; Santos, M. M.; Moutinho dos Santos, E. Energy Storage in the Energy Transition Context: A Technology Review. *Renewable Sustainable Energy Rev.* **2016**, *65*, 800−822.

(5) Equipment and Instruments or Materials Are Identified in the Paper to Adequately Specify the Experimental Details. Such Identification Does Not Imply Recommendation by the National Institute of Standards and Technology (NIST) nor Does It Imply That the Materials Are Necessarily the Best Available for the Purpose.

(6) Mauritz, K. A.; Moore, R. B. State of Understanding of Nafion. *Chem. Rev.* **2004**, *104*, 4535−4586.

(7) Tang, Z.; Keith, R.; Aaron, D. S.; Lawton, J. S.; Papandrew, A. P.; Zawodzinski, T. A., Jr. Proton Exchange Membrane Performance Characterization in VRFB. *ECS Trans.* **2012**, *41*, 25−34.
(8) Allen, F. I.; Comolli, L. R.; Kusoglu, A.; Modestino, M. A.; Minor, A. M.; Weber, A. Z. Morphology of Hydrated As-Cast Nafion Revealed through Cryo Electron Tomography. *ACS Macro Lett.* **2015**, *4*, 1−5.
(9) Dunn, B.; Kamath, H.; Tarascon, J.-M. Electrical Energy Storage for the Grid: A Battery of Choices. *Science* **2011**, *334*, 928−935.
(10) Davis, E. M.; Kim, J.; Oleshko, V. P.; Page, K. A.; Soles, C. L. Uncovering the Structure of Nafion-SiO_2 Hybrid Ionomer Membranes for Prospective Large-Scale Energy Storage Devices. *Adv. Funct. Mater.* **2015**, *25*, 4064−4075.
(11) Xi, J.; Wu, Z.; Qiu, X.; Chen, L. Nafion/SiO2 Hybrid Membrane for Vanadium Redox Flow Battery. *J. Power Sources* **2007**, *166*, 531−536.
(12) Mai, Z.; Zhang, H.; Li, X.; Xiao, S.; Zhang, H. Nafion/Polyvinylidene Fluoride Blend Membranes with Improved Ion Selectivity for Vanadium Redox Flow Battery Application. *J. Power Sources* **2011**, *196*, 5737−5741.
(13) Luo, Q.; Zhang, H.; Chen, J.; Qian, P.; Zhai, Y. Modification of Nafion Membrane Using Interfacial Polymerization for Vanadium Redox Flow Battery Applications. *J. Membr. Sci.* **2008**, *311*, 98−103.
(14) Kusoglu, A.; Weber, A. Z. New Insights into Perfluorinated Sulfonic-Acid Ionomers. *Chem. Rev.* **2017**, *117*, 987−1104.
(15) Teng, X.; Zhao, Y.; Xi, J.; Wu, Z.; Qiu, X.; Chen, L. Nafion/Organic Silica Modified TiO2 Composite Membrane for Vanadium Redox Flow Battery via in Situ Sol−Gel Reactions. *J. Membr. Sci.* **2009**, *341*, 149−154.
(16) Lin, C.-H.; Yang, M.-C.; Wei, H.-J. Amino-Silica Modified Nafion Membrane for Vanadium Redox Flow Battery. *J. Power Sources* **2015**, *282*, 562−571.
(17) Lu, S.; Wu, C.; Liang, D.; Tan, Q.; Xiang, Y. Layer-by-Layer Self-Assembly of Nafion−[CS−PWA] Composite Membranes with Suppressed Vanadium Ion Crossover for Vanadium Redox Flow Battery Applications. *RSC Adv.* **2014**, *4*, 24831−24837.
(18) Domhoff, A.; Balwani, A.; Martin, T. B.; Davis, E. M. Leveraging Nanoparticle Dispersion State To Tune Vanadium Ion Selectivity of Nanophase-Segregated Ionomer Nanocomposites for Redox Flow Batteries. *ACS Appl. Energy Mater.* **2019**, *2*, 8535−8549.
(19) Jansto, A.; Davis, E. M. Role of Surface Chemistry on Nanoparticle Dispersion and Vanadium Ion Crossover in Nafion Nanocomposite Membranes. *ACS Appl. Mater. Interfaces* **2018**, *10*, 36385−36397.
(20) Kondratenko, M. S.; Karpushkin, E. A.; Gvozdik, N. A.; Gallyamov, M. O.; Stevenson, K. J.; Sergeyev, V. G. Influence of Aminosilane Precursor Concentration on Physicochemical Properties of Composite Nafion Membranes for Vanadium Redox Flow Battery Applications. *J. Power Sources* **2017**, *340*, 32−39.
(21) Muriithi, B.; Loy, D. Proton Conductivity of Nafion/Ex-Situ Sulfonic Acid-Modified Stöber Silica Nanocomposite Membranes As a Function of Temperature, Silica Particles Size and Surface Modification. *Membranes* **2016**, *6*, No. 12.
(22) Sadhasivam, T.; Kim, H.-T.; Park, W.-S.; Lim, H.; Ryi, S.-K.; Roh, S.-H.; Jung, H.-Y. Low Permeable Composite Membrane Based on Sulfonated Poly(Phenylene Oxide) (SPPO) and Silica for Vanadium Redox Flow Battery. *Int. J. Hydrogen Energy* **2017**, *42*, 19035−19043.
(23) Teng, X.; Dai, J.; Su, J.; Zhu, Y.; Liu, H.; Song, Z. A High Performance Polytetrafluoroethene/Nafion Composite Membrane for Vanadium Redox Flow Battery Application. *J. Power Sources* **2013**, *240*, 131−139.
(24) Rabago, R.; Noble, R. D.; Koval, C. A. Effects of Incorporation of Fluorocarbon and Hydrocarbon Surfactants into Perfluorosulfonic Acid (Nafion) Membranes. *Chem. Mater.* **1994**, *6*, 947−951.
(25) Teng, X.; Dai, J.; Su, J.; Yin, G. Modification of Nafion Membrane Using Fluorocarbon Surfactant for All Vanadium Redox Flow Battery. *J. Membr. Sci.* **2015**, *476*, 20−29.
(26) Xiangguo, T.; Jicui, D.; Jing, S. Effects of Different Kinds of Surfactants on Nafion Membranes for All Vanadium Redox Flow Battery. *J. Solid State Electrochem.* **2015**, *19*, 1091−1101.
(27) Moore, C. M.; Hackman, S.; Brennan, T.; Minteer, S. D. Effects of Surfactants on the Transport Properties of Redox Species through Nafion Membranes. *J. Membr. Sci.* **2005**, *255*, 233−238.
(28) Mulmi, S.; Park, C. H.; Kim, H. K.; Lee, C. H.; Park, H. B.; Lee, Y. M. Surfactant-Assisted Polymer Electrolyte Nanocomposite Membranes for Fuel Cells. *J. Membr. Sci.* **2009**, *344*, 288−296.
(29) Park, C. H.; Kim, H. K.; Lee, C. H.; Park, H. B.; Lee, Y. M. Nafion Nanocomposite Membranes: Effect of Fluorosurfactants on Hydrophobic Silica Nanoparticle Dispersion and Direct Methanol Fuel Cell Performance. *J. Power Sources* **2009**, *194*, 646−654.
(30) Tricoli, V. Proton and Methanol Transport in Poly (Perfluorosulfonate) Membranes Containing Cs+ and H+ Cations. *J. Electrochem. Soc.* **1998**, *145*, 3798−3801.
(31) Liu, S.; Wang, L.; Ding, Y.; Liu, B.; Han, X.; Song, Y. Novel Sulfonated Poly (Ether Ether Keton)/Polyetherimide Acid-Base Blend Membranes for Vanadium Redox Flow Battery Applications. *Electrochim. Acta* **2014**, *130*, 90−96.
(32) Schneider, C. A.; Rasband, W. S.; Eliceiri, K. W. NIH Image to ImageJ: 25 Years of Image Analysis. *Nat. Methods* **2012**, *9*, 671−675.
(33) Kline, S. R. Reduction and Analysis of SANS and USANS Data Using IGOR Pro. *J. Appl. Crystallogr.* **2006**, *39*, 895−900.
(34) Bukola, S.; Liang, Y.; Korzeniewski, C.; Harris, J.; Creager, S. Selective Proton/Deuteron Transport through Nafion|Graphene|Nafion Sandwich Structures at High Current Density. *J. Am. Chem. Soc.* **2018**, *140*, 1743−1752.
(35) Shetzline, J. A.; Bukola, S.; Creager, S. E. A Convenient Miniature Test Platform for Polyelectrolyte Membrane Fuel-Cell Research. *J. Electroanal. Chem.* **2017**, *797*, 8−15.
(36) Semiz, L.; Sankir, N. D.; Sankir, M. Directly Copolymerized Disulfonated Poly(Arylene Ether Sulfone) Membranes for Vanadium Redox Flow Batteries. *Int. J. Electrochem. Sci.* **2014**, *9*, 3060.
(37) Lee, Y.; Kim, S.; Maljusch, A.; Conradi, O.; Kim, H.-J.; Jang, J. H.; Han, J.; Kim, J.; Henkensmeier, D. Polybenzimidazole Membranes Functionalised with 1-Methyl-2-Mesitylbenzimidazolium Ions via a Hexyl Linker for Use in Vanadium Flow Batteries. *Polymer* **2019**, *174*, 210−217.
(38) Peron, J.; Mani, A.; Zhao, X.; Edwards, D.; Adachi, M.; Soboleva, T.; Shi, Z.; Xie, Z.; Navessin, T.; Holdcroft, S. Properties of Nafion NR-211 Membranes for PEMFCs. *J. Membr. Sci.* **2010**, *356*, 44−51.
(39) Trogadas, P.; Pinot, E.; Fuller, T. F. Composite, Solvent-Casted Nafion Membranes for Vanadium Redox Flow Batteries. *Electrochem. Solid-State Lett.* **2012**, *15*, A5−A8.
(40) Gebel, G. Structure of Membranes for Fuel Cells: SANS and SAXS Analyses of Sulfonated PEEK Membranes and Solutions. *Macromolecules* **2013**, *46*, 6057−6066.
(41) Gebel, G.; Diat, O. Neutron and X-Ray Scattering: Suitable Tools for Studying Ionomer Membranes. *Fuel Cells* **2005**, *5*, 261−276.
(42) Ma, C.-H.; Yu, T. L.; Lin, H.-L.; Huang, Y.-T.; Chen, Y.-L.; Jeng, U.-S.; Lai, Y.-H.; Sun, Y.-S. Morphology and Properties of Nafion Membranes Prepared by Solution Casting. *Polymer* **2009**, *50*, 1764−1777.
(43) Dresch, M. A.; Matos, B. R.; Fonseca, F. C.; Santiago, E. I.; Carmo, M.; Lanfredi, A. J. C.; Balog, S. Small-Angle X-Ray and Neutron Scattering Study of Nafion-SiO2 Hybrid Membranes Prepared in Different Solvent Media. *J. Power Sources* **2015**, *274*, 560−567.
(44) Tang, Z.; Svoboda, R.; Lawton, J. S.; Aaron, D. S.; Papandrew, A. B.; Zawodzinski, T. A. Composition and Conductivity of Membranes Equilibrated with Solutions of Sulfuric Acid and Vanadyl Sulfate. *J. Electrochem. Soc.* **2013**, *160*, F1040−F1047.
(45) Wang, L.; Pingitore, A. T.; Xie, W.; Yang, Z.; Perry, M. L.; Benicewicz, B. C. Sulfonated PBI Gel Membranes for Redox Flow Batteries. *J. Electrochem. Soc.* **2019**, *166*, A1449.
(46) Lee, W.; Jung, M.; Serhiichuk, D.; Noh, C.; Gupta, G.; Harms, C.; Kwon, Y.; Henkensmeier, D. Layered Composite Membranes

Based on Porous PVDF Coated with a Thin, Dense PBI Layer for Vanadium Redox Flow Batteries. *J. Membr. Sci.* **2019**, *591*, No. 117333.

(47) Zhang, Y.; Li, J.; Wang, L.; Zhang, S. Sulfonated Polyimide/AlOOH Composite Membranes with Decreased Vanadium Permeability and Increased Stability for Vanadium Redox Flow Battery. *J. Solid State Electrochem.* **2014**, *18*, 3479−3490.

(48) Di Noto, V.; Lavina, S.; Negro, E.; Vittadello, M.; Conti, F.; Piga, M.; Pace, G. Hybrid Inorganic−Organic Proton Conducting Membranes Based on Nafion and 5wt% of MxOy (M = Ti, Zr, Hf, Ta and W). Part II: Relaxation Phenomena and Conductivity Mechanism. *J. Power Sources* **2009**, *187*, 57−66.

(49) Di Noto, V.; Gliubizzi, R.; Negro, E.; Pace, G. Effect of SiO2 on Relaxation Phenomena and Mechanism of Ion Conductivity of [Nafion/(SiO2)x] Composite Membranes. *J. Phys. Chem. B* **2006**, *110*, 24972−24986.

(50) Di Noto, V.; Piga, M.; Pace, G.; Negro, E.; Lavina, S. Dielectric Relaxations and Conductivity Mechanism of Nafion: Studies Based on Broadband Dielectric Spectroscopy. *ECS Trans.* **2019**, *16*, 1183.

https://dx.doi.org/10.1021/acs.macromol.0c01696
Macromolecules 2021, 54, 440−449